Two-way phase-shift time stepping for the acoustic wave equation

Ben D. Wards[1], *Gary F. Margrave*[1] *and Michael P. Lamoureux* [2]

ABSTRACT

We consider the time-stepping of a wavefield using a Fourier-domain phase shift as an alternative to the common finite-difference approach. For the acoustic wave-equation, we derive a time-stepping method that, like second-order (in time) finite differencing, uses two wavefield snapshots, one in the present and another one step in the past, to calculate a new snapshot one step in the future. Unlike finite-differencing, for homogeneous media our phase-shift time-stepping method is exact and displays no dispersion or instability if an aliasing condition is met. An aliasing condition, which we derive, limits the size of the possible time step. For heterogeneous media, we develop a windowed Fourier approximation, essentially a phase-shift in the Gabor domain, that is an approximate propagator with minimal numerical artifacts. This Gabor approximation represents the velocity variation through a chosen number, which directly controls computational effort, of reference velocities. For each reference velocity we describe the construction of the corresponding spatial windows such that the sum of all windows sums to unity. We demonstrate the potential of our method by performing prestack reverse-time migration of the Marmousi dataset and by a simple forward modeling example.

[1]University of Calgary, Department of Geoscience, CREWES (Consortium for Research in Elastic Wave Exploration Seismology), Calgary, Alberta, Canada. E-mail: bdwards@ucalgary.ca; margrave@ucalgary.ca.

[2]The University of Calgary,Department of Mathematics and Statistics, POTSI (Pseudodifferential Operator Theory & Seismic Imaging) Calgary, Alberta T2N 1N4, Canada E-mail: mikel@math.ucalgary.ca.

INTRODUCTION

Reverse-time migration (RTM) (Baysal et al., 1983; McMechan, 1983) is capable of imaging reflectors using all acoustic wave modes including overturned waves and multiples. However, as a result of the sampling requirements, processing seismic surveys with RTM will require either low-pass filtering to remove higher frequency data or long run times even with a cluster of computers. The fine sampling requirements occur because finite-difference operators have an approximate dispersion relation that becomes more incorrect with increasing time (Cohen, 2001). An example of the impressive performance, yet low frequency response, is given in Jones et al. (2007).

Seismic migration by phase-shift depth stepping (Gazdag, 1978) is accurate and efficient provided that there are no lateral velocity variations. Phase-shift-plus-interpolation (PSPI) was presented by Gazdag and Sguazzero (1984) as an approximate extension to lateral velocity variations. It spatially interpolates between a set of extrapolated wavefields corresponding to a set of reference velocities.

The principle of phase-shift depth stepping is based on approximating the two-way wave equation by a one-way wave equation about a preferred direction normally taken to be vertical. The resulting one-way wave equation is solved in the Fourier domain. While highly accurate for waves propagating in the preferred direction in a constant velocity medium, the approximation is inaccurate at steep dips and high lateral velocity contrast (e.g., de Hoop et al., 2000). The two-way wave equation, although more accurate, is more computationally intense and so has historically had limited use for seismic migration.

The concept of phase shift has been extended in the literature in order to better handle stability and accuracy when the velocity varies in the lateral direction (Stoffa et al., 1990; Wu and Huang, 1992; de Hoop et al., 2000). Margrave and Ferguson (1999) showed that the GPSPI (generalized phase-shift-plus-interpolation) Fourier integral is the limit of PSPI in the extreme case of using a distinct reference velocity for each output location. The Gabor method of windowed Fourier transforms can be used (Ma and Margrave, 2008) to approximate GPSPI by choosing a collection of reference velocities according to a error

criterion called lateral position error.

Returning to time-stepping, the Fourier domain has been used in pseudospectral methods to calculate the Laplacian of the wavefield. Usually, the finite-difference is used to estimate the time derivative of the wavefield thereby leading to a time marching scheme. The finite-difference approximation is dispersive while the Laplacian is computed with infinite order accuracy. However, as a result the numerical dispersion due to time differencing cannot be canceled with the numerical dispersion due to spatially differencing.

We investigate an alternative time-stepping equation that does not use finite-difference approximations. Our solution is based on the exact solution to the constant-velocity wave equation and it does not suffer from numerical dispersion. We show that our method is essentially a phase shift, dependent upon velocity and wavenumber, and call it phase-shift time-stepping or PSTS. The fundamental limitation on the timestep size in PSTS arises from a temporal aliasing condition, which we derive. The accuracy and stability properties are demonstrated by comparing solutions of the time-stepping equation to finite-difference solutions. We extend PSTS to variable velocity by replacing the global Fourier transform with a local Gabor transform using localizing windows within which a homogeneous solution is computed. This extension is no longer exact but still allows accurate time-stepping with minimal dispersion.

TWO-WAY TIME STEPPING BY A PHASE-SHIFT

The following conventions are used for the forward and inverse Fourier transform of the function $\varphi : \mathbb{R}^2 \to \mathbb{C}$,

$$\hat{\varphi}(\vec{k}) = \mathcal{F}_{\vec{x}\to\vec{k}}(\varphi) = \int_{\mathbb{R}^2} e^{2\pi i \vec{x}\cdot\vec{k}} \varphi(\vec{x}) dx dz, \tag{1}$$

and

$$\varphi(\vec{x}) = \mathcal{F}^{-1}_{\vec{k}\to\vec{x}}(\hat{\varphi}) = \int_{\mathbb{R}^2} e^{-2\pi i \vec{x}\cdot\vec{k}} \hat{\varphi}(\vec{k}) dk_x dk_z, \tag{2}$$

where $\mathbb{R}$ is the real line, $i = \sqrt{-1}$, $\vec{x} = (x, y, z) \in \mathbb{R}^3$, $\vec{k} = (k_x, k_y, k_z) \in \mathbb{R}^3$ is the Fourier domain coordinate conjugate to $\vec{x}$, and the hat denotes a Fourier transformed function of

the spacial coordinates. The symbols $\mathcal{F}_{\vec{x}\to\vec{k}}$, and $\mathcal{F}^{-1}_{\vec{k}\to\vec{x}}$ are used to denote the forward and inverse Fourier transforms as abstract operators, respectively. Later, the symbols $\mathcal{F}_{\vec{x}\to\vec{k}}$, and $\mathcal{F}^{-1}_{\vec{k}\to\vec{x}}$ are also used to denote the Fourier-like integrals when φ or $\hat{\varphi}$ depend upon $\vec{k}$ and $\vec{x}$ explicitly. In this case, a single FFT cannot be used to calculated the Fourier transform.

Common wave-equation depth migration methods recursively extrapolate the recorded wavefield downward in depth. In contrast, RTM, like forward modeling, recursively propagates the recorded wavefield in time. This is typically done by finite-differencing the two-way wave equation. As an alternative to finite-differencing the wave equation, our time-stepping equation is formulated by phase-shifting the Fourier transform of the wavefield with a cosine operator. The time-stepping equation is based on an exact solution of the constant-velocity wave equation,

$$\frac{\partial^2 U}{\partial t^2} = c^2 \left(\frac{\partial^2 U}{\partial x^2} + \frac{\partial^2 U}{\partial y^2} + \frac{\partial^2 U}{\partial z^2} \right), \tag{3}$$

where $U(t, \vec{x})$ is the amplitude of the wave at the point $(t, \vec{x} = (x, y, z))$, x, y are the lateral coordinate, z is the depth coordinate, t is the time coordinate, $\partial^2 U/\partial t^2$ is, for example, the second-order partial derivative of the wavefield with respect to the time coordinate, and c, a constant, is the speed of propagation. Assume $\vec{x} \in \mathbb{R}^3$ and $t \in \mathbb{R}$.

Applying the Fourier transform over the spatial dimensions $\vec{x} = (x, y, z)$ to both sides of equation (3), reduces it to a collection of ordinary differential equations,

$$\frac{\partial^2 \hat{U}}{\partial t^2} = -(2\pi)^2 c^2 \left(k_x^2 + k_y^2 + k_z^2 \right) \hat{U}. \tag{4}$$

Equation (4) is not equivalent to (3) when the velocity is spatially dependant. When $\vec{k} \neq 0$, equation (4) has the general solution

$$\hat{U}(t, \vec{k}) = A(\vec{k}) \cos(2\pi\omega(\vec{k})t) + B(\vec{k}) \sin(2\pi\omega(\vec{k})t), \tag{5}$$

where $A(\vec{k})$ and $B(\vec{k})$ are dependent on the initial conditions, and the wavenumber depen-

dent frequency, ω, is determined from the dispersion relation

$$\omega(\vec{k}) = c\sqrt{k_x^2 + k_y^2 + k_z^2}. \tag{6}$$

When $\vec{k} = 0$, the solution is identically zero provided that the initial wavefield and its derivative are integrable funtions. After the functions A and B are specified, the space-domain solution may be calculated by taking an inverse Fourier transform. Subject to the initial conditions

$$\begin{cases} U(0, \vec{x}) = f(\vec{x}) \\ U(-\delta t, \vec{x}) = g(\vec{x}) \end{cases}, \tag{7}$$

where δt denotes a timestep, the functions A and B are determined by

$$\begin{cases} A(\vec{k}) = \hat{f}(\vec{k}) = \hat{U}(0, \vec{k}) \\ B(\vec{k})\sin(2\pi\omega\delta t) = \hat{f}(\vec{k})\cos(2\pi\omega\delta t) - \hat{g}(\vec{k}) \end{cases}. \tag{8}$$

The resulting exact solution at time $t = \delta t$ of constant velocity wave equation is

$$U(\delta t, \vec{x}) = -U(-\delta t, \vec{x}) + 2\mathcal{F}^{-1}_{\vec{k}\to\vec{x}}[\cos(2\pi\omega(\vec{k})\delta t)\mathcal{F}_{\vec{x}\to\vec{k}}[U(0, \vec{x})]]. \tag{9}$$

The fast Fourier transform can be employed to compute equation (9) because the kernel of the Fourier integral is independent of the spatial coordinate $\vec{x}$. We may interpret equation (9) as a sum of two phase shifts, not a cascade, since

$$2\cos\left(2\pi\omega(\vec{k})\delta t\right) = \exp\left(-2\pi i\omega(\vec{k})\delta t\right) + \exp\left(2\pi i\omega(\vec{k})\delta t\right). \tag{10}$$

Equation (9) is the fundamental equation for PSTS (phase-shift time stepping) and we will soon adapt it to variable velocity.

To demonstrate the effectiveness of recursively using equation (9) for wavefield propagation, a minimum phase wavelet is stepped forward in time. The minimum phase wavelet is injected at the center point of a constant velocity 2D model at the start of propagation. Figure 1 is the propagation of a minimum phase wavelet using the phase-shift time-stepper

and also with conventional second-order finite differencing. In spite of a much smaller timestep, the finite-difference solution shows unacceptable distortion due to numerical grid dispersion.

ALIASING

Equation (9) is exact for constant velocity. With sampled data the size of the timestep for equation (9) is limited by aliasing considerations. Equation (9) takes snapshots of the wavefield at two distinct times with spatial sampling rate δx and generates a new wavefield snapshot at a future time. The wavenumber which corresponds to the greatest frequency occurs when $(k_x, k_y, k_z) = \left(\pm\frac{\pi}{\delta x}, \pm\frac{\pi}{\delta x}, \pm\frac{\pi}{\delta x}\right)$, the Nyquist wavenumbers. By the dispersion relation, the maximum wavenumber generates a frequency $\omega = \pi c\sqrt{3}/\delta x$. Since the wavefield is sampled in time at rate δt, the Nyquist frequency is $\omega = \pi/\delta t$. Thus $r = \delta t\, c/\delta x$ must satisfy the inequality $r < 1/\sqrt{3}$ to avoid aliasing. A similar inequality is also required to be satisfied by finite difference solvers depending on the order but additionally 10 samples per wave length to propagate with low amount of dispersion rather than the 2 samples per wave length for equation (9). Figure 2 shows how aliasing starts at $r = 1/\sqrt{2}$ in the case of two spatial dimensions.

TIMESTEPPING IN A VARIABLE-VELOCITY MEDIUM

The variable-velocity acoustic wave equation is

$$\frac{\partial^2 U}{\partial t^2} = v^2(x,y,z)\left(\frac{\partial^2 U}{\partial x^2} + \frac{\partial^2 U}{\partial y^2} + \frac{\partial^2 U}{\partial z^2}\right), \tag{11}$$

where $v(x,y,z)$ is the spatially dependent velocity. We now adapt equation (9) which propagates an acoustic wavefield exactly in a constant velocity medium to propagate approximately in a variable velocity medium. Equation (11) has a local causality property which means that the wavefield $U(t,\vec{x})$ only depends on the wavefield locally. As a result, the right hand side of equation (11), $v^2(\vec{x})\,(U_{xx} + U_{yy} + U_{zz})$, can, for small enough δt, be approximated locally near $\vec{x}_0$ by the solution to the frozen term $v^2(\vec{x}_0)\,(U_{xx} + U_{yy} + U_{zz})$.

This means that by replacing the constant velocity appearing in the dispersion relation in equation (9) by the variable velocity (i.e. unfreezing the velocity), we have an approximate solution

$$U(\delta t, \vec{x}) = -U(-\delta t, \vec{x}) + 2\mathcal{F}^{-1}_{\vec{k}\to\vec{x}}\left[\cos\left(2\pi v(\vec{x})|\vec{k}|\delta t\right)\mathcal{F}_{\vec{x}\to\vec{k}}\left[U(0,\vec{x})\right]\right]. \tag{12}$$

This is the freezing-unfreezing argument that appears in the literature in the context of hyperbolic and elliptic partial differential equations e.g., (p. 230-231, Stein, 1993). Such solutions are often called locally homogeneous approximations (e.g., Ma and Margrave, 2008) and they approximate the solution to the variable velocity wave equation by the solution locally from the constant velocity wave equation. In fact the local homogenous approximation is used for both finite-difference and pseudospectral solvers.

Equation (12), for variable velocity, is too numerically complex to be used directly for wavefield propagation. We use a Gabor windowing scheme to approximate it and so the resulting operator is a Gabor multiplier. The Gabor Transform is a windowed Fourier transform. Equation (12) is a Fourier integral operator (Stein, 1993). Numerical computation of these operators is an active area of research (Candès et al., 2007). Please refer to Appendix A for various definitions of terms that occur in this section.

A 2-D partition of unity (POU, see again Appendix A) is used to partition the velocity model into N regions with approximate constant velocity, $v_j, j \in [1, N]$, called reference velocities. In our method these regions need not be simply connected. The wavefield in each region is then propagated with the corresponding reference velocity. Figure 3 is an example velocity partition, or window, used to migrate the Marmousi data set. It is apparent that our constant velocity regions have very complex shape. Their construction is detailed in the next section. The POU is used to window the wavefield into regions at each timestep and the combination of windowing and Fourier transformation results in the Gabor approximation to equation (9) given by

$$U(\delta t, \vec{x}) = -U(-\delta t, \vec{x}) + \sum_{j=1}^{N} 2\mathcal{F}^{-1}_{\vec{k}\to\vec{x}}\left[\cos\left(2\pi\omega_j\delta t\right)\mathcal{F}_{\vec{x}\to\vec{k}}\left[\Omega_j(\vec{x})U(0,\vec{x})\right]\right], \tag{13}$$

where $\omega_j(k_x, k_y, k_z) = v_j\sqrt{k_x^2 + k_y^2 + k_z^2}$, and v_j is the reference velocity used for propagation in the jth window $\Omega_j(\vec{x})$.

It is possible to write equation (13) more explicitly as a Gabor multiplier. If $g_j = \Omega_j$, $\gamma_j = 1$, and the Gabor multiplier $M_j(\vec{k}) = \cos(2\pi\omega_j\delta t)$, then

$$\begin{aligned} U(\delta t, \vec{x}) &= -U(-\delta t, \vec{x}) + \sum_{j=1}^{N} \gamma_j \mathcal{F}^{-1}_{\vec{k}\to\vec{x}} \left[M_j(\vec{k}) \mathcal{F}_{\vec{x}\to\vec{k}} \left[g_j U(0, \vec{x}) \right] \right], \\ &= -U(-\delta t, \vec{x}) + \sum_{j=1}^{N} V^{-1}_{\gamma_j} \left[M_j V_{g_j} \left[U(0, \vec{x}) \right] \right], \end{aligned} \tag{14}$$

where $V_{g_j}[U(0, \vec{x})](\vec{k})$ is the forward Gabor transform (as defined in Appendix A) applied to the function $U(0, \vec{x})$ and $V^{-1}_{\gamma_j}$ is the inverse Gabor transform.

Equation (9) can be computed efficiently because at each timestep two three-dimensional fast Fourier transform (FFT) are computed. This means the numerical complexity is $n_x \log(n_x) n_y \log(n_y) n_z \log(n_z)$ where n_x, n_y, n_z are the number of points used to discretize the x, y, z variable, respectively. For variable velocity the number of FFTs required significantly increase. For the Marmousi dataset 20 FFTS are required for reasonable accuracy. For equation (12) the FFT can not be used so that the numerical complexity at each timestep is $n_z^2 n_y^2 n_x^2$. For PSTS the grid spacing can be much more coarse and correspondingly the timestep as compared to low order finite difference. Higher-order pseudospectral methods require a slightly smaller gridspacing because time derivative is approximated but significantly fewer FFTs are computed.

CONSTRUCTING GABOR ANALYSIS WINDOWS AND VELOCITY APPROXIMATIONS

The computational complexity of the PSTS equation depends linearly on the number of reference velocities used to approximate the velocity model. Constructing accurate approximations with a minimal number of referencee velocities allows numerically efficient phase-shift timestepping algorithms. Methods for choosing reference velocities are found in, for

example, Bagaini et al. (1995) or Ma and Margrave (2008). A simple method is to take the reference velocities equally spaced between the lowest and greatest velocity. However if there is an uneven distribution of velocities or if there is a particular commonly occurring velocity in the medium it may be desired to clump the reference velocities. An alternative approach is to choose simultaneously the reference velocities,v_j, and the corresponding spatial windows, $\Omega_j(\vec{x})$, so that they minimize the L_2 error $||v(\vec{x}) - \sum_{j=1}^{N} v_j \Omega_j(\vec{x})||_{L^2}$, where $||f(\vec{x}))||_{L^2} = \left(\int_{\mathbb{R}^2} |f(x,y,z)|^2 dxdydz\right)^{1/2}$ is the common L_2 norm. In the present context, we simply assume that suitable reference velocities have been obtained and describe the construction of the corresponding spatial windows.

To construct the POU $\{\Omega_1(\vec{x}), \ldots, \Omega_N(\vec{x})\}$ given a set of reference velocities $\{v_1, \ldots, v_N\}$, we first construct a simpler POU based on discontinuous indicator functions $\{I_1(\vec{x}), \ldots, I_N(\vec{x})\}$ where

$$I_j(\vec{x}) = \begin{cases} 1 & : \quad |v_j - v(\vec{x})| \text{ is a minimum for } j \in [1, N] \\ 0 & : \quad \text{otherwise} \end{cases} \tag{15}$$

where the meaning of the right-hand side is that the indicator function is only unity when $|v_j - v(\vec{x})|$ assumes a minimum for the j^{th} reference velocity, and is otherwise zero. Also, the nature of the functions $\{I_j(\vec{x})\}$ is such that they will generally have multiple, disconnected maxima. Given this discontinuous POU, we can construct a smooth POU by a normalized convolution with a suitable bump function or *atomic window*. Suppose that $\theta : \mathbb{R}^2 \to \mathbb{R}$ is a positive smooth function localized at $\vec{x} = 0$. For example θ could be a Gaussian function $\exp\left(-x^2/2\sigma^2\right)$ for a particular value of σ which determines the degree of smoothing. Then

$$\Omega_j = \frac{\theta * I_j}{\sum_{k=1}^{N} \theta * I_k}, j = 1, \ldots, N \tag{16}$$

defines a smooth partition of unity, where $*$ denotes a 2D spatial convolution. Figure 3 shows both the I_j and Ω_j windows corresponding to a single reference velocity used to migrate the Marmousi data set.

The window set $\{\Omega_1, \ldots, \Omega_N\}$ works well with RTM as the resulting velocity approxi-

mation

$$v_{smooth}(\vec{x}) = \sum_{j=1}^{N} v_j \Omega_j(\vec{x}) \tag{17}$$

is naturally smooth and acts to suppress unwanted internal reflections. Usually such reflections are not desired and simply add noise to the final image. However, if the location of the reflector is known with accuracy, it may be desirable to retain a velocity discontinuity representing it because this allows the accurate migration of associated multiples. A velocity approximation which tends to retain velocity discontinuities can be constructed using the indicator functions, rather than the smooth windows, as

$$v_{discrete}(\vec{x}) = \sum_{j=1}^{N} v_j I_j(\vec{x}), \tag{18}$$

which we will employ later in a modeling example.

PSEUDOSPECTRAL METHODS

Finite-difference methods and pseudospectral methods have been gained wide spread acceptance for modeling and migration. We compare them with the PSTS equation. The pseudospectral method uses the Fourier transform over the spacial coordinates to numerically calculate the Laplacian. The second-time derivative is approximated by the second-order centered finite-difference operator to derive a time-marching algorithm

$$U^{n+1} = 2U^n - U^{n-1} - \delta t^2 v^2 \mathcal{F}^{-1}_{\vec{k}\to\vec{x}}[(2\pi|\vec{k}|)^2 \mathcal{F}_{\vec{x}\to\vec{k}}[U^n]], \tag{19}$$

where the superscripts n refers to the approximation at timestep n. To deduce a higher-order algorithm, a higher-order finite-difference approximation can be used for the second-time derivative of U. However these algorithms are unconditionally unstable (Cohen, 2001). Alternatively, the modified equation approach or the Lax-Wendroff method (Cohen, 2001)

can be used. The Taylor series expansion of the second-order time derivative is

$$\left(\frac{\partial^2 U}{\partial t^2}\right)^n = \frac{U^{n+1} - 2U^n + U^{n-1}}{\delta t^2} - \frac{\delta t^2}{12}\left(\frac{\partial^4 U}{\partial t^4}\right)^n + O(\delta t^6) \tag{20}$$

which is derived by adding together the Taylor series expansion of $U(t+\delta t)$ and $U(t-\delta t)$ about t. The wave equation can be used to approximate the higher order time derivatives, e.g.,

$$\frac{\partial^4 U}{\partial t^4} \simeq v^4 \Delta(\Delta U).$$

Substituting equation (20) into the scalar wave equation gives the fourth-order time approximation,

$$U^{n+1} = \delta t^2 v^2 (\Delta U)^n - U^{n-1} + 2U^n + \frac{v^4 \delta t^4}{12}\left(\Delta^2 U\right)^n + \ldots, \tag{21}$$

where ΔU refers to the Laplacian of the function U and $\Delta^2 U$ is the biharmonic or the Laplacian applied twice to U. If a higher-order expansion in equation (21) is used then formally (Etgen, 1989; Dablain, 1986; Chen, 2007),

$$U^{n+1} = -U^{n-1} + 2\sum_{k=0}^{\infty} \frac{(\delta t v)^{2k}}{(2k)!}\left(\Delta^k U\right)^n. \tag{22}$$

Taking the Fourier transform of both sides of equation (22) with respect to the spatial coordinates,

$$\begin{aligned} \widehat{U}^{n+1} &= -\widehat{U}^{n-1} + 2\sum_{k=0}^{\infty} \frac{(\delta t v)^{2k}}{(2k)!}\left((-2\pi|\vec{k}|)^{2k}\widehat{U}\right)^n \\ &= -\widehat{U}^{n-1} + 2\cos\left(2\pi v|k|\delta t\right)\widehat{U}^n. \end{aligned} \tag{23}$$

The second-order in time pseudospectral method can be derived formally from equation (12) by replacing the cosine function by its second-order power series expansion. Thus equation (12) clearly generalizes the pseudospectral method and therefore finite-difference schemes as well and, for homogeneous media, is superior.

Equation (23) could in principle be used to for wavefield propagation, however, it is

too computationally expensive. Instead it is desirable to find a sum of functions of $\vec{x}$ and $\vec{k}$ separately. Soubaras and Zhang (2008) use an equiripple polynomial to approximate $\cos(2\pi v|k|\delta t)$ instead of a Taylor series approximation which is used to derive the higher-order pseudospectral method. Etgen and Brandsberg-Dahl (2009) approximates (23) by interpolate between two cosine propagators,

$$\begin{aligned} U^{n+1} = -U^{n-1} &+ 2\frac{v_H^2 - v^2(\vec{x})}{v_H^2 - v_L^2}\mathcal{F}^{-1}_{\vec{k}\to\vec{x}}\{\cos(2\pi v_L|k|\delta t)\,\widehat{U}^n\} \\ &+ 2\frac{v^2(\vec{x}) - v_L^2}{v_H^2 - v_L^2}\mathcal{F}^{-1}_{\vec{k}\to\vec{x}}\{\cos(2\pi v_H|k|\delta t)\,\widehat{U}^n\}. \end{aligned} \tag{24}$$

When the cosines are expanded with a Taylor series expansion the method is at least as accurate as fourth-order in time pseudospectral method through its benefits are more for suppression of shear wave artifacts in pseudo-acoustic anisotropy wavefield propagators. Tal-Ezer (1986) expands the cosine with orthogonal systems of Chebyshev polynomials and Bessel functions and proves that this is optimal.

THE MARMOUSI DATA SET

The Marmousi data set (Versteeg, 1994) is a common benchmark to test migration algorithms. Although it does not showcase the strengths of RTM, e.g. the imaging overturned reflectors, it does allow us to demonstrate that PSTS RTM can image seismic data in a complex medium.

To benchmark PSTS RTM we compare it to a second-order time and fourth-order space finite-difference RTM. The PSTS method uses the velocity model of equation 17 where $N = 18$ reference velocities where chosen. Figure 4 is a comparison of two snapshots of the forward modeled shot using the PSTS algorithm and a second-order finite-difference algorithm. The numerical noise is greater in the finite-difference solution and there are subtle differences in amplitude along the wavefront. Slightly different velocity models are used for propagation because the model of equation 17 does not perfectly match the exact model which was used in the finite difference case. Figure 5 is the PSTS prestack depth migration result and Figure 8 is the finite-difference result. Both of these results are the

composite stack of all 240 migrated shot records comprising the Marmousi dataset. While grossly similar, the two images are different in detail almost everywhere. Our purpose is not to establish the superiority of one method over the other but rather to present evidence that phase-shift methods can accomplish wavefield time stepping in highly heterogeneous media. The PSTS RTM result was calculated using a coarser spatial grid and a larger timestep than the finite-difference method. For the PSTS the spatial grid spacing was 12.5 meters in both directions and the time step was $1.5ms$. To prevent spatial aliasing the shot field and receiver field were resampled to a grid spacing of $6.25m$ prior to applying the imaging condition. For the finite difference RTM the grid spacing was $5m$ and the timestep was taken to be $0.3ms$. A single shot took twice as long with a low-order finite difference approach as compared with the PSTS equation.

A MODELING EXAMPLE

Migration is commonly done with a smooth velocity field where the approximation works well, however, for the modeling of reflections the discontinuities in the velocity field are very important. Here we approximate the velocity field as in equation 18 by using indicator functions which have a discontinuous step at a reflector. Unlike the RTM algorithm presented above, the indicator windows are not smoothed to suppress reflections but they still sum to unity. Again we use equation (12) but now as a modeling algorithm to test the ability of the PSTS equation to generate reflections. Figure 9 compares finite differencing to the PSTS equation for forward modeling in a three layer medium. The PSTS result is non-dispersive and compares well to the finite-difference result. We have not attempted to compare the reflection amplitudes in this example, either with each other or with theory. However, this suggests that there is potential either for modeling with PSTS or to include certain multiple generating horizons in RTM.

CONCLUSION

We proposed a Fourier domain phase-shift equation for time-stepping wavefields and called the resulting algorithm PSTS (phase-shift time-stepping). Our method multiplies the spatial Fourier transform of the wavefield by a cosine whose argument depends on velocity and wavenumber. The variable velocity PSTS equation is a Fourier integral operator whose direct computation is very slow. We presented a computationally feasible approximation to this operator using a spatial Gabor transform with windows that adapt to the velocity structure. The number of windows chosen, one for each *reference velocity*, directly controls the computational speed and must be minimized. We also gave prescriptions to produce Gabor-approximate velocity models that either are naturally smooth or that preserve discontinuities. We demonstrated the potential to use PSTS for RTM by migrating the Marmousi data set with a smooth velocity approximation. We showed that the PSTS image compares well with a more conventional finite-difference result. PSTS can use a much larger timestep and a coarser spatial grid than a typical finite-difference method. We also briefly examined the potential to use a discontinuous velocity approximation to model reflections. The result is comparable to that obtained by finite-differencing.

ACKNOWLEDGEMENTS

We thank the sponsors of the CREWES project, and those of the POTSI consortium, and especially NSERC, MITACS, PIMS, and Alberta Ingenuity.

APPENDIX: THE 2D GABOR TRANSFORM AND ADAPTIVE PARTITIONS OF UNITY

The Fourier transform has been used extensively in seismic signal processing as a method of filtering and for wavefield continuation migrations (e.g. Gazdag (1978); Stolt (1978)). However, seismic signals and operators change character over space and time requiring a time variant or space variant filtering (Margrave, 1998). For wavefield continuation migrations, the Fourier transform methods lose their efficiency as the velocity model becomes

more complex. As an alternative to the Fourier transform or as a generalization of it, the Gabor transform has been used to deal with the nonstationary character of seismic signals. It was first proposed by Gabor (1946) as the windowing of a signal with a space shifted Gaussian function, followed by a Fourier transform, and then repeated for many window positions. The Gabor transform has been used successively in seismic imaging to implement nonstationary filters. For example, Margrave et al. (2005) proposed Gabor deconvolution which corrects the data for anelastic attenuation. While Ma and Margrave (2008), and Grossman et al. (2002) have proposed highly accurate Gabor depth imaging algorithms.

To solve the wave equation in a variable velocity medium, we approximate the velocity function using a partition of unity (POU). A POU is a suite of window functions $\{\Omega_j(\vec{x}) : \mathbb{R}^2 \to [0,1], j \in [1,N]\}$ satisfying

$$1 = \sum_{j=1}^{N} \Omega_j(\vec{x}), \tag{A-1}$$

where each $\Omega_j(\vec{x})$ is usually, but not necessarily, a smooth function bounded between 0 and 1. Given a velocity model $v(\vec{x})$ that is a piecewise continuous function defined on a compact set or constant off a compact, then for any $\epsilon > 0$ there exists an N and a POU

$$\{\Omega_j(\vec{x}) : \mathbb{R}^2 \to [0,1], j \in [1,N]\} \tag{A-2}$$

and a collection of corresponding reference velocities v_j so that

$$\left|\left| \sum_{j=1}^{N} v_j \Omega_j(\vec{x}) - v(\vec{x}) \right|\right|_{L^2} < \epsilon. \tag{A-3}$$

In contrast to the mathematical definition, we allow the POU to be non smooth. The POU can be used to define a Gabor analysis and synthesis window pair. Let $g_j(\vec{x}) = \Omega_j^p(\vec{x})$ and $\gamma_j(\vec{x}) = \Omega_j^{1-p}(\vec{x})$ for any $p \in [0,1]$. The functions $\{g_j, j = 1, \ldots, M\}$ are called analysis windows, while the functions $\{\gamma_j, j = 1, \ldots, N\}$ are called synthesis windows. When $p = 0$, or 1 the analysis windows, or synthesis widows are unity, respectively. The forward Gabor transform is defined by

$$V_g \psi_j(\vec{k}) = \mathcal{F}_{\vec{x} \to \vec{k}}[g_j(\vec{x})\psi(\vec{x})]. \tag{A-4}$$

An inverse to the Gabor transform operating on the Gabor spectra $W(\vec{k}, j)$ is defined by

$$V_\gamma^{-1} W(\vec{k}, j) = \sum_j \gamma_j(\vec{x}) \mathcal{F}^{-1}_{\vec{k}\to\vec{x}}[W(\vec{k}, j)], \tag{A-5}$$

as

$$\begin{aligned} V_\gamma^{-1} V_g \psi_j(\vec{x}) &= \sum_j \gamma_j(\vec{x}) \mathcal{F}^{-1}_{\vec{k}\to\vec{x}}[V_g \psi_j(\vec{x})] \\ &= \sum_j \gamma_j(\vec{x}) \mathcal{F}^{-1}_{\vec{k}\to\vec{x}} \mathcal{F}_{\vec{x}\to\vec{k}}[g_j(\vec{x})\psi(\vec{x})] \\ &= \sum_j \gamma_j(\vec{x}) g_j(\vec{x}) \psi(\vec{x}) \\ &= \sum_j \Omega_j(\vec{x}) \psi(\vec{x}) \\ &= \psi(\vec{x}). \end{aligned} \tag{A-6}$$

In general, the inverse to the Gabor transform is not unique, but the above definition is easy to compute and enjoys good numerical properties. For wavefield propagation the cases $p = 0, 1$ are usually preferred. This is because the cases $p \in (0, 1)$ take twice as long to compute.

A Gabor multiplier is the Gabor transform equivalent of a Fourier multiplier or filter. The Gabor spectrum is multiplied pointwise by a time-frequency or space-wavenumber filter. The inverse of the new spectrum is calculated to obtain the nonstationary filtered signal. Specifically, a Gabor multiplier, is the triple (g, γ, M) where for a function $\psi : \mathbb{R}^2 \to \mathbb{R}$ suitably defined,

$$M_{g,\gamma} \psi = V_\gamma^{-1} M V_g \psi. \tag{A-7}$$

In general the action of the Gabor multiplier depends upon the windowing functions.

REFERENCES

Bagaini, C., E. Bonomi, and E. Pieroni, 1995, Data parallel implementation of 3-D PSPI: 65nd Ann. Internat.Mtg., Soc. Expl. Geophys., Expanded Abstracts,, **188-191**.

Baysal, E., D. D. Kosloff, and J. W. C. Sherwood, 1983, Reverse time migration: Geo-

physics, **48**, 1514–1524.

Candès, E., L. Demanet, and L. Ying, 2007, Fast computation of Fourier integral operators: SIAM J. Sci. Comput., **29**, 2464–2493.

Chen, J.-B., 2007, High-order time discretizations in seismic modeling: Geophysics, **72**, SM115–SM122.

Cohen, G. C., 2001, Higher-order numerical methods for transient wave equations: Springer Verlag.

Dablain, M. A., 1986, The application of high-order differencing to the scalar wave equation: Geophysics, **51**, 54–66.

de Hoop, M. V., J. H. L. Rousseau, and R.-S. Wu, 2000, Generalization of the phase-screen approximation for the scattering of acoustic waves: Wave Motion, **31**, 43 – 70.

Etgen, J., 1989, Accurate wave equation modeling: SEP–60.

Etgen, J. T., and S. Brandsberg-Dahl, 2009, The pseudo-analytical method: Application of pseudo-laplacians to acoustic and acoustic anisotropic wave propagation: SEG Technical Program Expanded Abstracts, **28**, 2552–2556.

Gabor, D., 1946, Theory of communication: Journal of the Institute of Electrical Engineers, **93**, 429–457.

Gazdag, J., 1978, Wave equation migration with the phase-shift method: Geophysics, **43**, 1342–1351.

Gazdag, J., and P. Sguazzero, 1984, Migration of seismic data by phase shift plus interpolation: Geophysics, **49**, 124–131.

Grossman, J., G. Margrave, and M. P. Lamoureux, 2002, Constructing adaptive, nonuniform Gabor frames from partitions of unity: CREWES Research Report 14.

Jones, I. F., M. C. Goodwin, I. D. Berranger, H. Zhou, and P. A. Farmer, 2007, Application of anisotropic 3D reverse time migration to complex north sea imaging: SEG Technical Program Expanded Abstracts, **26**, 2140–2144.

Ma, Y., and G. F. Margrave, 2008, Seismic depth imaging with the Gabor transform: Geophysics, **73**, S91–S97.

Margrave, G. F., 1998, Theory of nonstationary linear filtering in the Fourier domain with application to time-variant filtering: Geophysics, **63**, 244–259.

Margrave, G. F., and R. J. Ferguson, 1999, Wavefield extrapolation by nonstationary phase shift: Geophysics, **64**, 1067–1078.

Margrave, G. F., P. C. Gibson, J. P. Grossman, D. C. Henley, V. Iliescu, and M. P. Lamoureux, 2005, The Gabor transform, pseudodifferential operators, and seismic deconvolution: Integr. Comput.-Aided Eng., **12**, 43–55.

McMechan, G. A., 1983, Migration by extrapolation of time-dependent boundary values: Geophysical Prospecting, **31**, 413–420.

Soubaras, R., and Y. Zhang, 2008, Two-step explicit marching method for reverse time migration: SEG Technical Program Expanded Abstracts, **27**, 2272–2276.

Stein, E., 1993, Harmonic analysis : real-variable methods, orthogonality, and oscillatory integrals: Princeton University Press.

Stoffa, P. L., J. T. Fokkema, R. M. de Luna Freire, and W. P. Kessinger, 1990, Split-step Fourier migration: Geophysics, **55**, 410–421.

Stolt, R. H., 1978, Migration by Fourier transform: Geophysics, **43**, 23–48.

Tal-Ezer, H., 1986, Spectral methods in time for hyperbolic equations: SIAM J. Numer. Anal., **23**, 11–26.

Versteeg, R., 1994, The Marmousi experience; velocity model determination on a synthetic complex data set: The Leading Edge, **13**, 927–936.

Wu, R.-S., and L.-J. Huang, 1992, Scattered field calculation in heterogeneous media using a phase-screen propagator: SEG Technical Program Expanded Abstracts, **11**, 1289–1292.

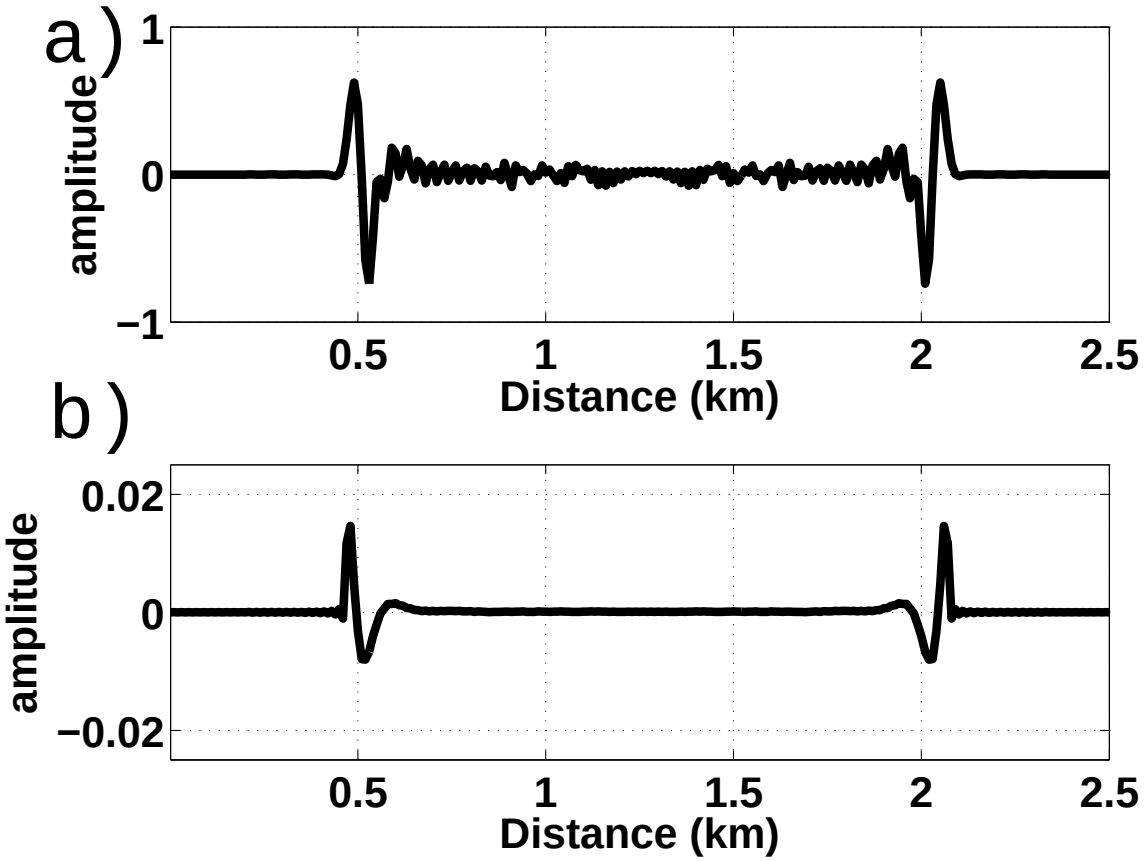

Figure 1: Cross sectional view through center of a 2D model with constant velocity model injected with a minimum phase wavelet. (a) Using finite differences with $\delta t = 0.0001$. (b) Using the phase-shift time-stepping equation with $\delta t = 0.001$. The low-order finite-difference timestepper took 10 times as long to execute.

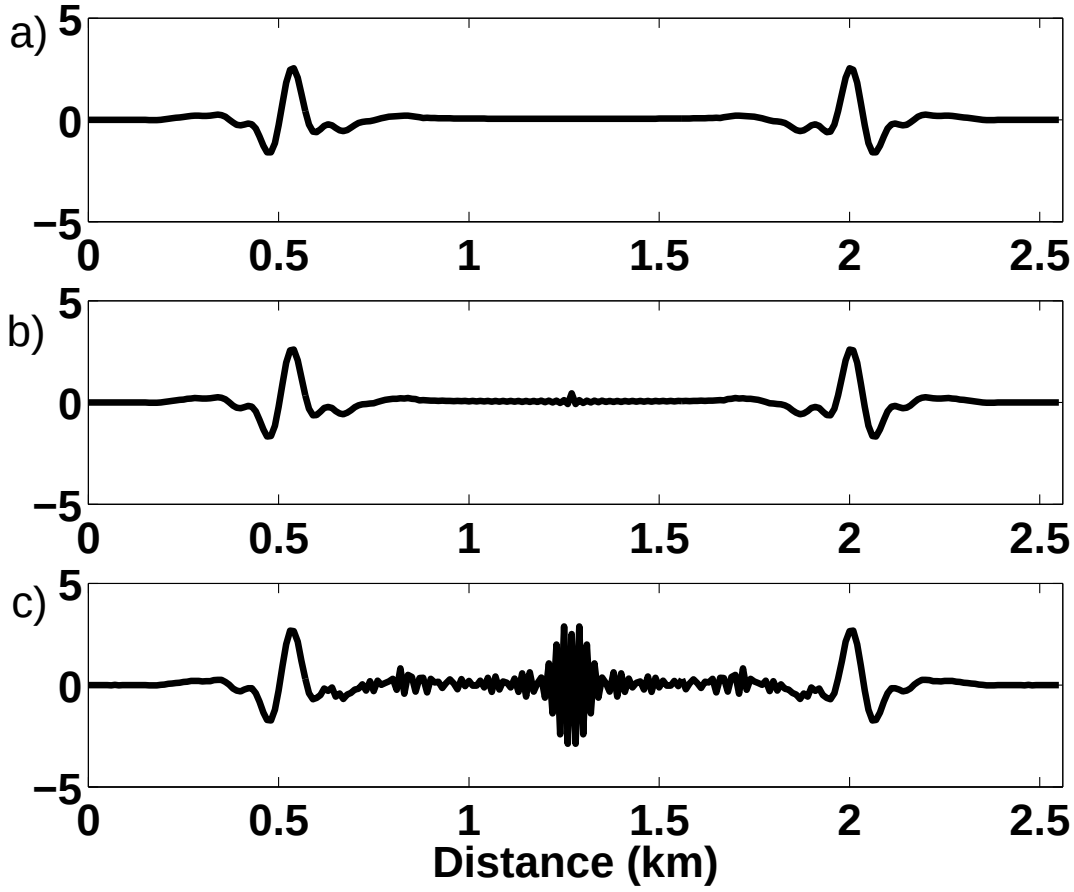

Figure 2: Cross sectional view of the response to zero phase wavelet injected at the center of a constant velocity model and forward propagated for various values of the aliasing number r. When $r > \sqrt{(1/2)}$ aliasing occurs in the model. From top to bottom $r = 0.68 \leq 0.71$, $r = 1.00 \not\leq 0.71$, and $r = 1.5 \not\leq 0.71$, respectively. The grid spacing was taken to be a constant, $10m$, and the time step was varied for the constant velocity, $v = 2500m/s$. The maximum frequency in the wavelet was $35Hz$.

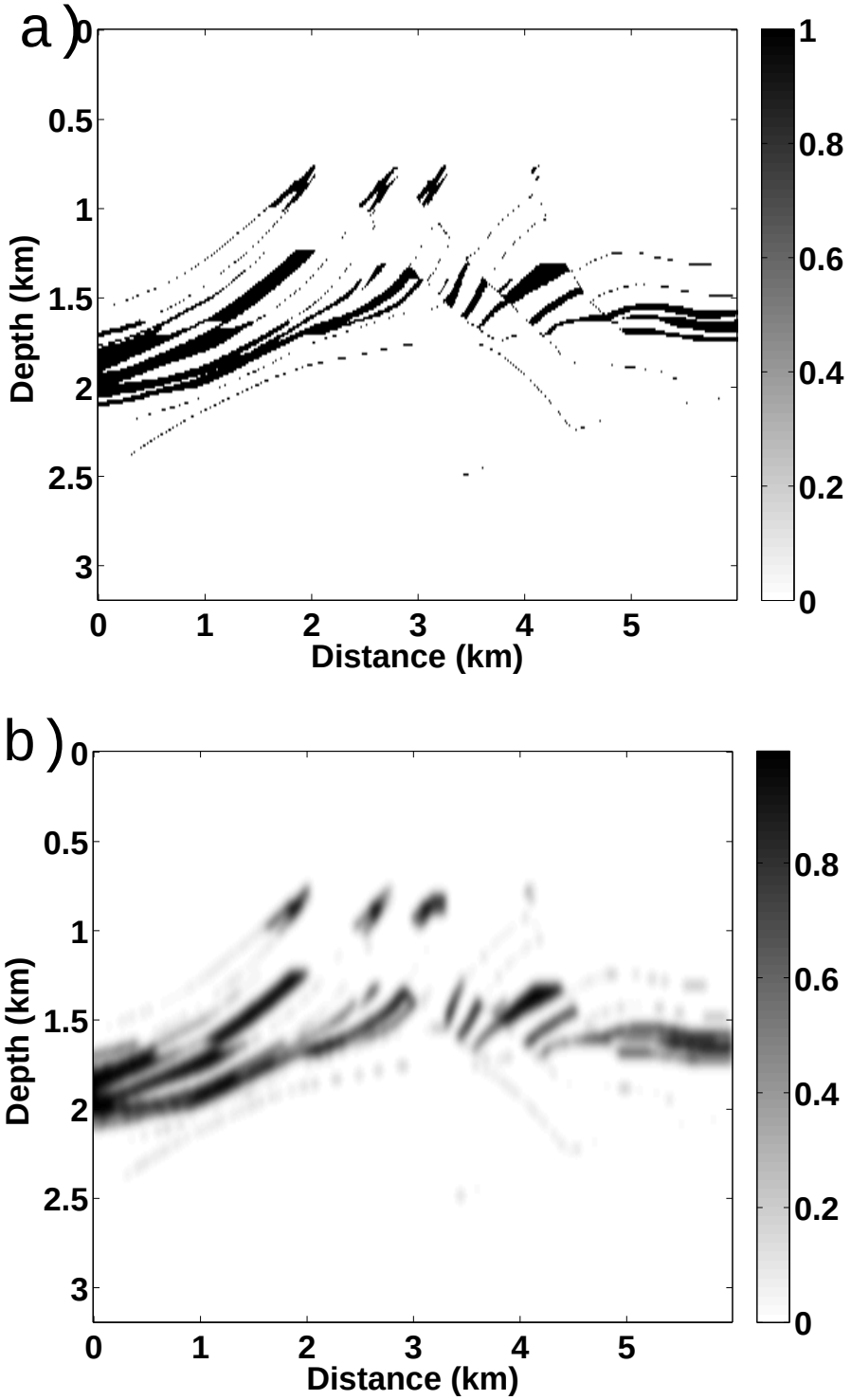

Figure 3: (a) An indicator function I_j corresponding to one of the reference velocities used to migrate the Marmousi data set. (b) The corresponding smoothed window Ω_j.

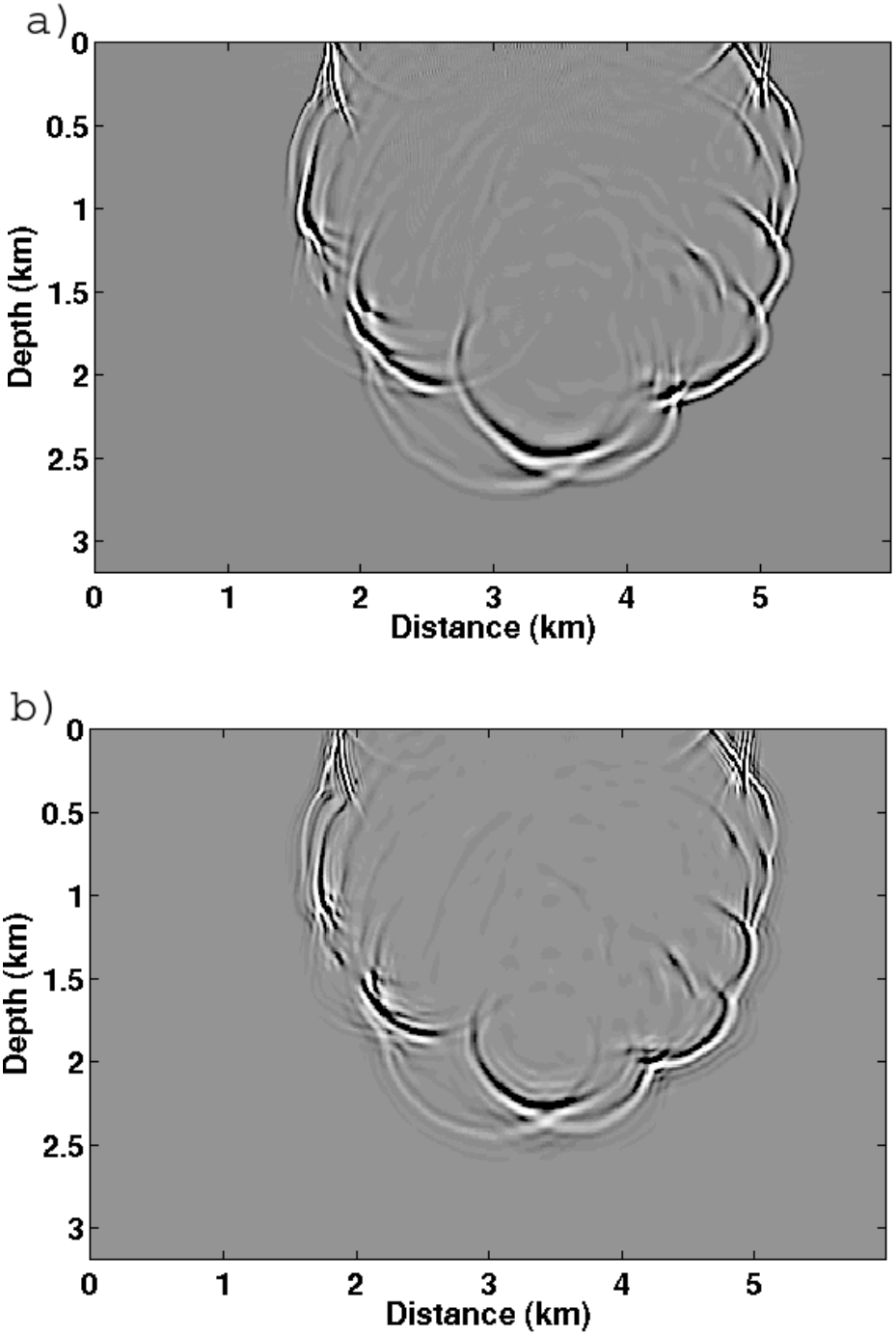

Figure 4: (a) A snapshot of the shot field propagated using PSTS for variable velocity. (b) A snapshot of the shot field propagated by finite-differencing the wave equation.

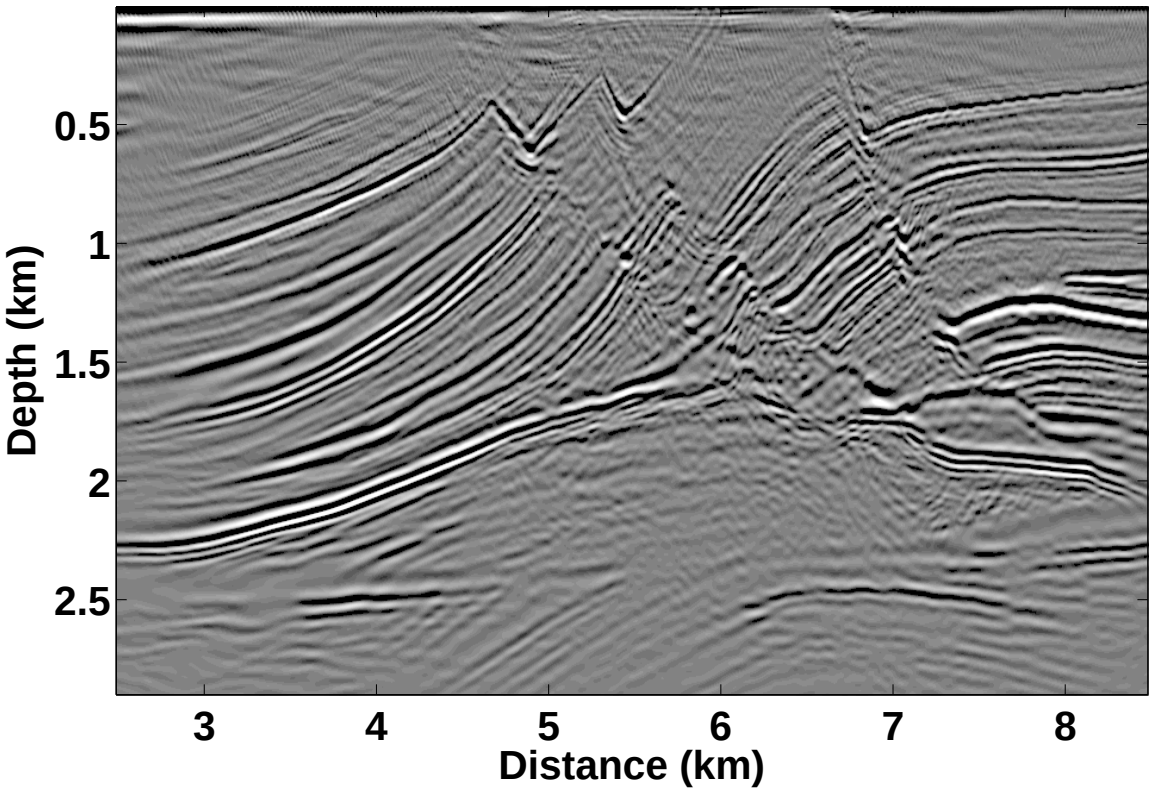

Figure 5: An image the Marmousi data set using PSTS RTM. The image is the stack of 240 migrated shot records. The timestep was 0.0015ms and the grid spacing was 12.5m. An error criteria was used (40m/s) which produced 18 reference velocities.

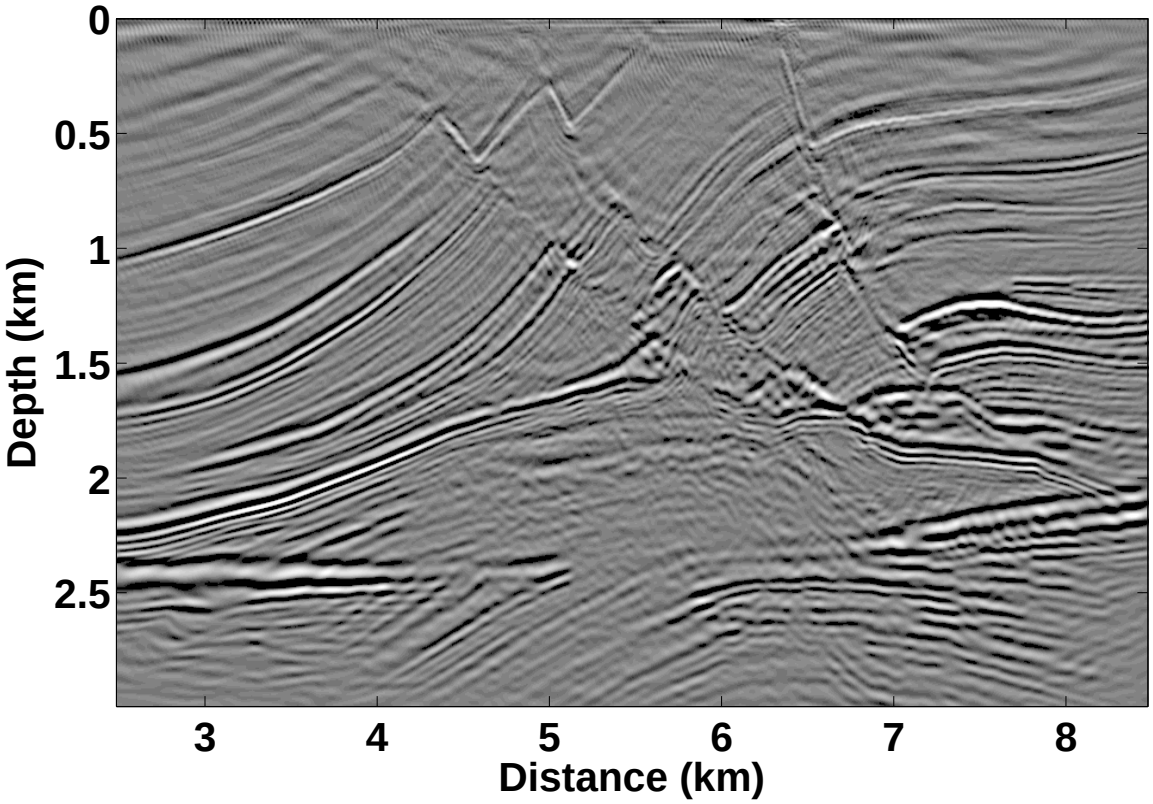

Figure 6: Similar to Figure 5 except that the migration method was second-order time and fourth-order space explicit finite-difference RTM. The timestep was 0.0003s and the grid spacing was 5m. This required about twice the computational effort of Figure 5.

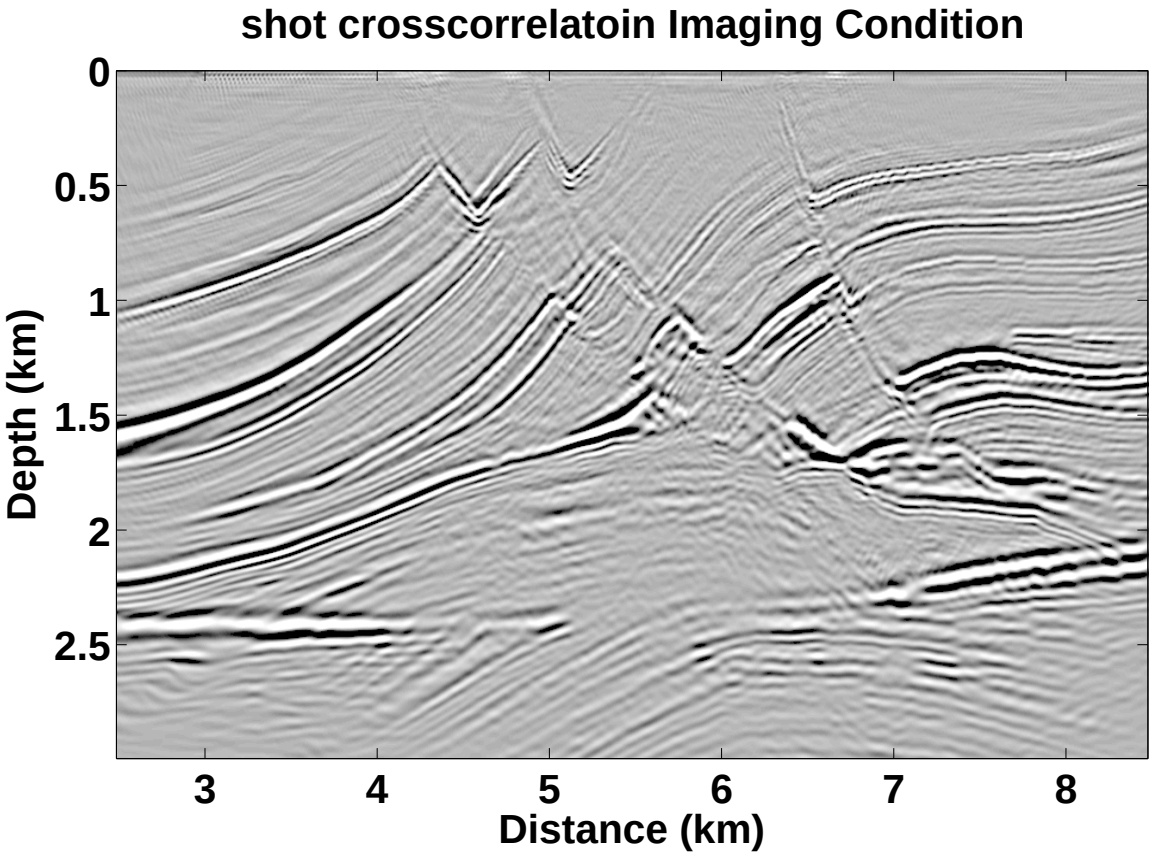

Figure 7: Similar to Figure 5 except that the migration method was second-order time and fourth-order space explicit finite-difference RTM. The timestep was 0.0003s and the grid spacing was 5m. This required about twice the computational effort of Figure 5.

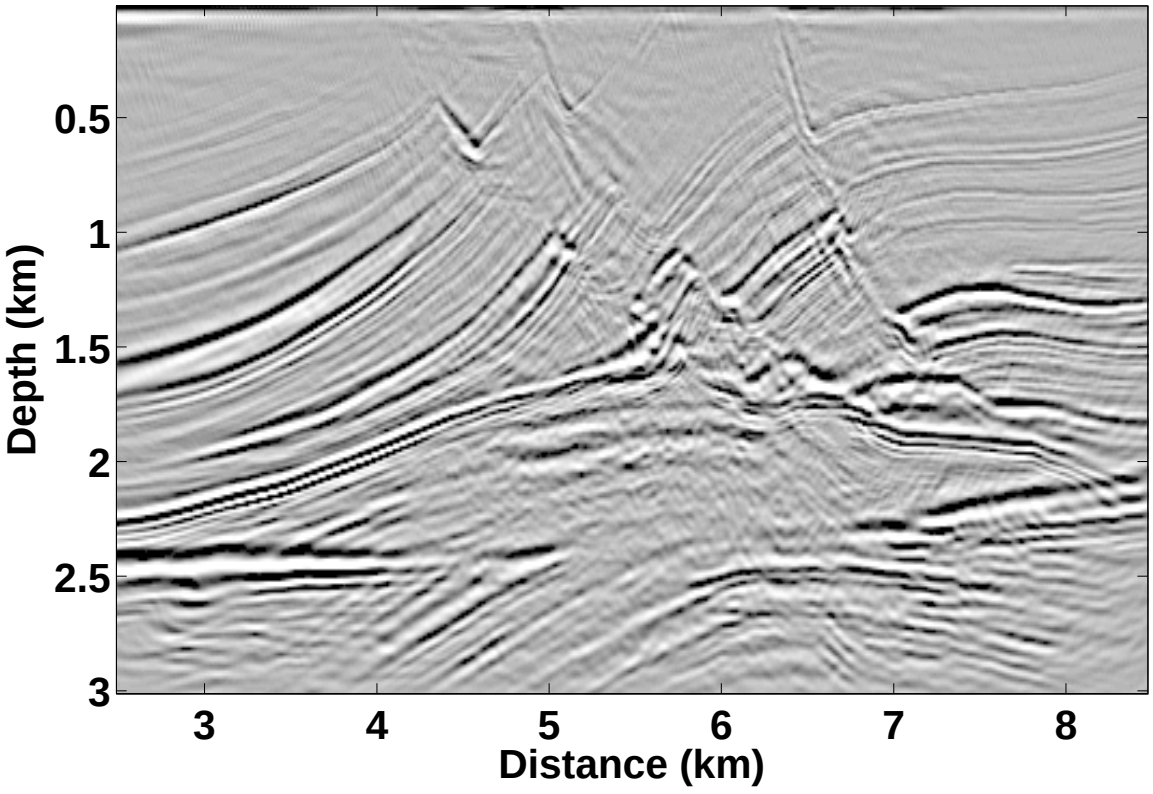

Figure 8: pseudo4

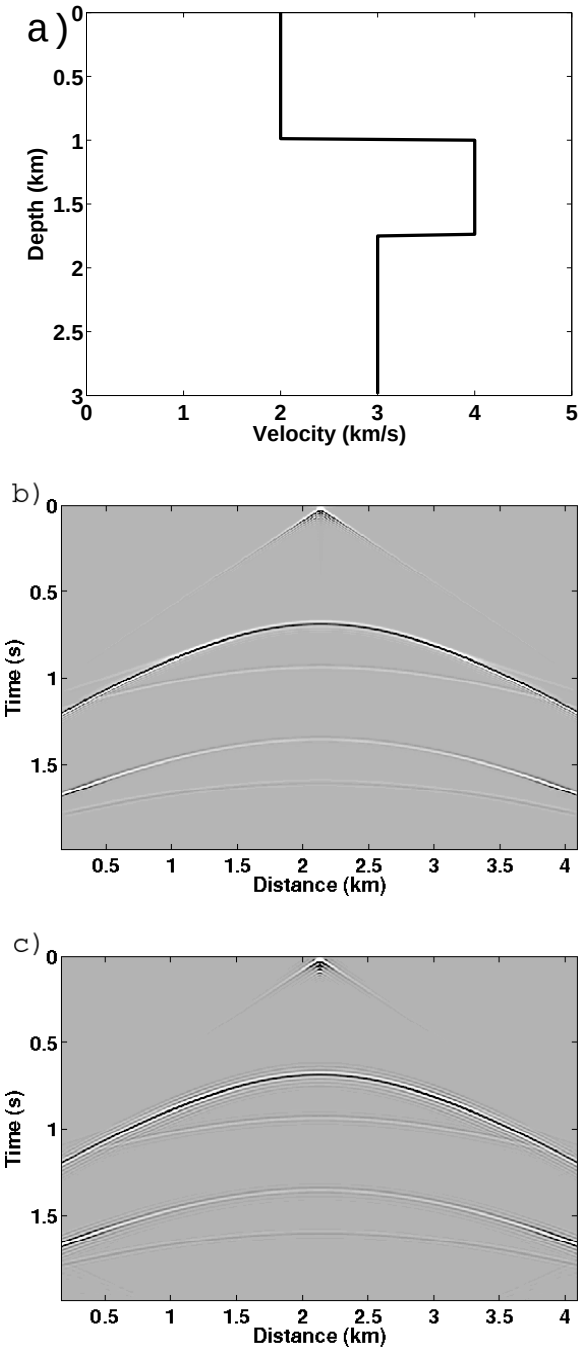

Figure 9: (a) Velocity profile for a 2D 3 layer velocity model. (b) shot record using the PSTS equation with non-smoothed windows. (c) Shot record using second-order time fourth-order space finite differences.